Dicle University
Journal of Engineering
https://dergipark.org.tr/tr/pub/dumf
duje.dicle.edu.tr

Research Article

Dynamical Analysis and Robust Chaos Suppression of the Newton-Leipnik System via Sliding Mode Control

Mert Süleyman DEMİRSOY[1*], Yusuf HAMİDA EL NASER[2]

[1] Sakarya University of Applied Sciences, Department of Mechatronics Engineering, mertdemirsoy@subu.edu.tr, ORCID: 0000-0002-7905-2254
[2] Sakarya University of Applied Sciences, Department of Mechatronics Engineering, yusufelnaser@subu.edu.tr, ORCID: 0000-0003-4757-6288

ARTICLE INFO

Article history:

Received 4 June 2026
Received in revised form 10 July 2026
Accepted 22 July 2026
Available online 7 August 2026

Keywords:

Chaos analysis, Sliding mode control, Newton-Leipnik system

Doi: 10.24012/dumf.1964154

* Corresponding author

ABSTRACT

This study presents the analysis and robust control of the Newton-Leipnik chaotic system within a nonlinear dynamical systems framework. The system is formulated parametrically and examined through time responses, phase portraits, Lyapunov exponents, and bifurcation analysis to identify its chaotic characteristics and parameter-dependent behavior. The results confirm that the uncontrolled system exhibits bounded but aperiodic motion, a strange attractor, and clear sensitivity to initial conditions, indicating a fully developed chaotic regime. Following the dynamical analysis, a sliding mode control strategy is designed to suppress chaotic oscillations and regulate all state variables to the equilibrium point. A complete Lyapunov stability analysis is derived for disturbance-free and disturbed cases, providing an explicit gain condition and a closed-form ultimate bound. The controller is then evaluated under nominal and disturbed conditions. Simulation results show that the control law rapidly stabilizes the system, eliminates chaotic behavior, and maintains bounded control effort. To assess robustness, the closed-loop response is tested under impulsive and oscillatory disturbances. In both cases, the controller preserves stability, quickly restores the system to the desired operating region, and yields state deviations that agree with the analytically predicted ultimate bound to four significant digits. Transient performance measures and the ISE, IAE, ITAE, and RMSE indices are reported in tabular form, while the influence of the switching function on chattering is quantified by comparing sign, saturation, and hyperbolic tangent alternatives. The findings demonstrate that sliding mode control provides a reliable and robust solution for stabilizing the Newton-Leipnik chaotic system, and that the proposed framework offers a useful basis for future studies on robust chaos suppression and nonlinear control design.

Introduction

Chaos theory has become a fundamental framework for understanding nonlinear deterministic systems whose trajectories exhibit irregular, aperiodic, and apparently random behavior despite being governed by deterministic equations. A defining characteristic of chaotic systems is sensitive dependence on initial conditions, meaning that arbitrarily small differences in initial states may lead to exponentially diverging trajectories over time [1–4]. This property distinguishes chaos from stochastic randomness and makes chaotic dynamics particularly important in systems where long-term prediction, stability, and control are critical. Historically, the development of chaos theory has been strongly associated with nonlinear dynamical systems, strange attractors, bifurcation mechanisms, and numerical simulation-based analysis [1,3,5].

The mathematical characterization of chaos is commonly based on phase-space analysis, attractor structures, bifurcation diagrams, Lyapunov exponents, fractal dimensions, and entropy-related measures [1,3,4]. Among these tools, Lyapunov exponents are widely used to quantify the average exponential divergence of nearby trajectories, while phase portraits and bifurcation diagrams provide qualitative insight into the transition from regular to chaotic motion. However, the diagnosis of chaos is not always straightforward. Some studies emphasize that a positive largest Lyapunov exponent is a useful indicator of chaotic behavior, whereas others argue that chaos identification should not rely on a single criterion alone but should instead be supported by complementary dynamical evidence such as bifurcation structure and attractor geometry [3,6]. Therefore, reliable analysis of chaotic systems generally requires the combined use of numerical, geometric, and stability-based methods.

Another important aspect of chaos theory is the transition mechanism from regular motion to chaotic behavior. Period-doubling cascades, intermittency, quasiperiodicity, and torus breakdown are among the most frequently discussed routes to chaos [2–4]. The period-doubling route, in particular, has been associated with universal scaling properties and Feigenbaum constants, indicating that different nonlinear systems may exhibit similar transition patterns under parameter variation [1, 2]. More advanced studies have also investigated critical dynamics at the onset of chaos, generalized statistical mechanics, renormalization-group approaches, and complex-network representations of chaotic time series [7–9]. In addition, the distinction between chaotic, quasiperiodic, and strange nonchaotic attractors has shown that fractal geometry and dynamical instability are not always equivalent properties [10,11]. These developments demonstrate that chaos theory provides not only a descriptive language for irregular motion but also a rigorous analytical basis for classifying nonlinear dynamical behavior.

The relevance of chaos theory extends across many scientific and engineering domains. Atmospheric dynamics, cardiovascular systems, biological networks, cancer modeling, power electronics, robotic systems, and electrical machines have all been investigated using concepts such as attractors, bifurcations, Lyapunov exponents, and nonlinear stability [3,12–14]. Recent studies have also demonstrated that chaotic control strategies can be effectively transferred from theoretical nonlinear systems to practical engineering applications. Demirsoy et al. proposed a chaotic magnetic stirrer in which the magnetic stir bar position was continuously varied according to Halvorsen, Lorenz, and Sprott-A chaotic equations, resulting in faster saturation and improved dissolution performance compared with conventional magnetic stirring [15]. Similarly, El Naser et al. implemented Sprott-A-based chaotic speed control for a DC motor-driven robotic end-effector mixer using MATLAB/Simulink, OrCAD, and STM32F407 hardware, showing that the selected chaotic signal could provide stable PWM-based motor control and reduced vibration [16]. Sarıkaya et al. investigated chaotic speed-controlled mixing in a biogas reactor and reported improved methane production and combustion duration compared with fixed-speed mixing, particularly under Sprott-A-based chaotic control [17]. These studies indicate that chaotic signals can be used not only for theoretical analysis and synchronization but also as practical control inputs for improving mixing efficiency, motor-driven actuation, and process performance in real engineering systems.

In engineering systems, chaotic behavior may lead to undesirable oscillations, instability, degraded performance, and sensitivity to disturbances. For this reason, the control of chaotic systems has become an important research field at the intersection of nonlinear dynamics and control theory. In this context, chaos control aims to suppress chaotic oscillations, stabilize equilibrium points or periodic orbits, synchronize chaotic systems, or, in some cases, intentionally generate complex chaotic motion for engineering applications.

Control studies on chaotic systems generally employ nonlinear and robust control methods because chaotic dynamics are highly sensitive to initial conditions, system parameters, and external disturbances. Lyapunov-based control, adaptive control, backstepping control, intermittent control, active control, and sliding mode control have been widely applied to stabilize or synchronize chaotic systems [18–21]. Among these methods, sliding mode control (SMC) is particularly attractive due to its robustness against parameter uncertainties, nonlinearities, and bounded disturbances. Recent studies have shown that SMC-based approaches can effectively regulate chaotic systems and achieve synchronization even in complex nonlinear models such as Lorenz-type chaotic systems and fractional-order memristive chaotic systems [18,22].

Synchronization is another major objective in chaos control studies. In this approach, a response system is forced to follow the trajectory of a drive chaotic system by designing a suitable controller that drives the synchronization error to zero. This concept has been widely used in secure communication, analog chaotic circuits, supply-chain dynamics, and nonlinear engineering models [19,23–25]. In addition to synchronization, chaos suppression has also been investigated through feedback, coupling, and delay-based strategies. Some studies have demonstrated that properly designed feedback or coupling mechanisms can transform chaotic behavior into steady or periodic motion, while others have used control laws to generate multi-scroll or hyperchaotic attractors for applications such as encryption and complex signal generation [26–28]. These studies indicate that chaos control is not limited to eliminating irregular behavior; rather, it provides a flexible framework for shaping nonlinear dynamics according to the desired engineering objective.

Within this broad research area, the Newton–Leipnik system represents an important class of continuous-time chaotic systems due to its nonlinear structure, rich dynamical behavior, and suitability for testing nonlinear control algorithms. Its sensitivity to initial conditions and complex attractor structure make it an appropriate benchmark for evaluating the effectiveness of robust control strategies. Although many studies have focused on the analysis and control of well-known chaotic systems such as Lorenz, Chen, Sprott-A, Halvorsen, and other multi-wing attractor models, further investigation is still needed for the systematic derivation, dynamical analysis, and robust control of Newton–Leipnik-type chaotic dynamics.

Motivated by this need, the present study focuses on the mathematical derivation and sliding mode control of the Newton–Leipnik chaotic system. First, the nonlinear dynamic model is formulated and its chaotic characteristics are investigated using phase portraits and time-domain responses. Then, an SMC strategy is designed to suppress chaotic oscillations and force the system states to converge toward the desired reference values. The proposed control structure is evaluated through numerical simulations, and the results demonstrate the effectiveness of the designed controller in stabilizing the chaotic Newton–Leipnik dynamics under nonlinear operating conditions.

Although the Newton–Leipnik system and sliding mode control are each well established individually, the specific contributions of this study are the following. (i) The system is formulated in a parametric form in which m is retained as a free bifurcation parameter, and the chaotic regime at $m = 5$ is established quantitatively through the complete Lyapunov spectrum, the negative sum of the exponents and the Kaplan–Yorke dimension, rather than being assumed. (ii) A complete Lyapunov stability analysis is derived both for the disturbance-free case and for the disturbed case, yielding an explicit gain condition and a closed-form ultimate bound which is subsequently verified against the simulation data. (iii) Robustness is assessed under two structurally different disturbance classes, an impulsive Gaussian perturbation and a persistent sinusoidal excitation, and is quantified through transient performance measures and the ISE, IAE, ITAE and RMSE indices. (iv) The chattering behaviour is examined explicitly by comparing the discontinuous sign function with the boundary-layer saturation and hyperbolic-tangent approximations, and the resulting trade-off between switching activity and steady-state accuracy is quantified.

Mathematical formulation and simulation setup

This section presents the mathematical formulation and numerical analysis framework of the Newton–Leipnik chaotic system. The governing nonlinear differential equations are first introduced, and the system is expressed in a parametric form to enable both dynamical analysis and bifurcation investigation. In particular, the system parameter m is retained as a variable to examine its influence on the transition between different dynamical regimes. To characterize the system behavior, a comprehensive set of analysis tools is employed, including time series, phase portraits, Lyapunov exponents, and bifurcation diagrams. These tools provide complementary insights into the qualitative and quantitative properties of the system, such as stability, sensitivity to initial conditions, and the emergence of chaotic dynamics. Time series analysis is used to observe the temporal evolution of the state variables, while phase portraits reveal the geometric structure of system trajectories in the state space. Lyapunov exponents are calculated to quantify the degree of chaos by measuring the exponential divergence of nearby trajectories, and bifurcation diagrams are constructed to investigate the effect of the control parameter m on the system dynamics.

All simulations are performed using MATLAB, where the nonlinear system is solved numerically due to the absence of closed-form analytical solutions. A high-accuracy numerical integration method is employed to ensure reliable representation of the system dynamics over a sufficiently long-time horizon. The selected initial conditions and parameter values are chosen to capture both transient and steady-state chaotic behavior, forming the basis for subsequent control design and performance evaluation.

System equations

The Newton–Leipnik system is a well-known continuous-time nonlinear dynamical system that exhibits rich chaotic behavior under specific parameter conditions. Due to its nonlinear coupling structure and sensitivity to initial conditions, it has been widely used as a benchmark model in chaos theory and nonlinear control studies.

In this study, the Newton–Leipnik system is considered in the following parametric form:

$$\begin{aligned} \dot{x} &= -0.4x + y + 10yz \\ \dot{y} &= -x - 0.4y + mxz \\ \dot{z} &= 0.175z - 5xy \end{aligned} \tag{1}$$

where x, y and z represent the system state variables, and m is a system parameter that plays a critical role in determining the dynamical behavior of the system, as shown in Equation (1).

Unlike fixed-parameter formulations commonly used in the literature, the parameter m is deliberately retained as a variable in this study to enable bifurcation analysis and to investigate the transition between different dynamical regimes. By varying m, the system can exhibit a wide range of behaviors, including stable equilibrium, periodic oscillations, and chaotic motion. In particular, the value $m = 5$ is selected as a reference operating point in which the system demonstrates fully developed chaotic dynamics.

The initial conditions of the system are defined as:

$$(x_0, y_0, z_0) = (0.349, 0, -0.16) \tag{2}$$

as given in Equation (2). These initial values are chosen to ensure that the system evolves toward the chaotic attractor and to provide consistency in comparative analyses across different simulation scenarios.

From a structural perspective, the system given in Equation (1) consists of both linear and nonlinear interaction terms. The linear terms ($-0.4x$, $-0.4y$, and $0.175z$) govern the local expansion and contraction of the flow. It should be noted that the term $0.175z$ is expanding rather than damping; the system is nevertheless dissipative because the trace of the Jacobian, $-0.4 - 0.4 + 0.175 = -0.625$, is negative, so that phase-space volumes contract uniformly. This value coincides with the sum of the Lyapunov exponents reported in the following section, which provides a consistency check on the numerical results. The nonlinear coupling terms (yz, xz, and xy) are responsible for the generation of complex and chaotic dynamics. The interplay between these components leads to the formation of a bounded yet irregular trajectory in the state space, which is a defining characteristic of chaotic systems.

This mathematical formulation serves as the foundation for the subsequent dynamical analysis, including time series evaluation, phase-space representation, Lyapunov exponent calculation, and bifurcation analysis. Furthermore, it provides the basis for the design and implementation of the sliding mode control strategy presented in the following sections.

Time series analysis

The time-domain behavior of the Newton–Leipnik system is analyzed to evaluate the dynamical characteristics of the state variables under the selected parameter value m=5 and the initial condition given in Equation (2). The time series of the state variables x_t, y_t and z_t obtained from the numerical solution of Equation (1) are presented in Figure 1.

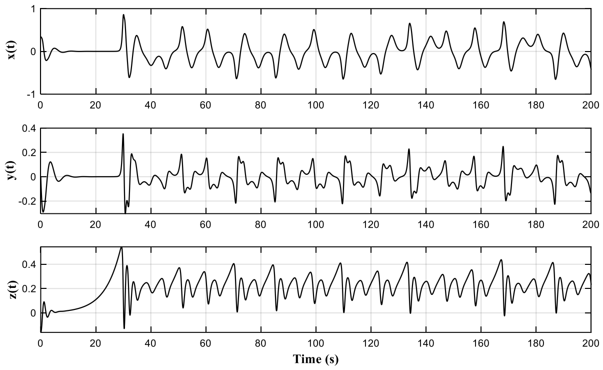

Figure 1. Time series of the Newton–Leipnik system state variables.

As shown in Fig. 1, the system exhibits irregular, aperiodic, and bounded oscillatory behavior, which is a fundamental indicator of chaotic dynamics. None of the state variables converge to a steady-state equilibrium or display periodic repetition over time. Instead, the trajectories evolve in a complex and non-repeating manner, confirming that the system operates in a chaotic regime.

It can be observed that the system initially undergoes a transient phase approximately within the interval $t = 0$ to $t \approx 30$, during which the state variables adjust from the initial conditions toward the attractor region. After this transient period, the system transitions into a fully developed chaotic state, where the oscillations become more irregular and exhibit pseudo-random characteristics.

A comparison of the state variables reveals distinct dynamical features. The x_t state demonstrates relatively higher amplitude fluctuations and sharper transitions, indicating a stronger influence of nonlinear coupling terms. In contrast, y_t exhibits smaller amplitude variations but still maintains irregular oscillatory behavior. The z_t state shows comparatively smoother transitions, yet it preserves the non-periodic nature of the system. These differences arise from the asymmetric structure of the nonlinear interaction terms in Equation (1). Another important observation from Fig. 1 is that all state variables remain bounded within a finite range despite their irregular behavior. This boundedness indicates that the trajectories evolve on a strange attractor rather than diverging to infinity, which is a key requirement for physical realizability and subsequent control design. Furthermore, the irregular and non-repeating structure of the time series suggests a broad frequency content, which is typical for chaotic systems. This property implies that the system cannot be effectively characterized using simple harmonic components and highlights the limitations of classical linear analysis techniques.

Time series analysis confirms that the Newton–Leipnik system, as defined in Equation (1) with $m = 5$, exhibits fully developed chaotic behavior. These results provide a necessary foundation for further dynamical analysis, including phase-space investigation, Lyapunov exponent calculation, and bifurcation analysis, as well as for the design of robust control strategies such as sliding mode control.

Phase portraits

To further investigate the dynamical behavior of the Newton–Leipnik system, phase portraits are analyzed in both two-dimensional and three-dimensional state spaces. The phase-space trajectories obtained from the numerical solution of Equation (1) are illustrated in Figure 2.

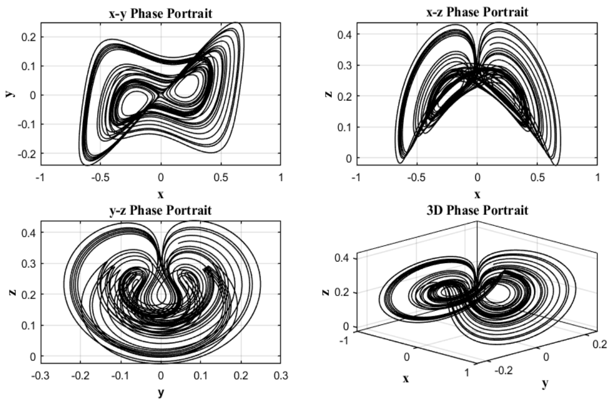

Figure 2. Phase portraits of the Newton–Leipnik system.

As shown in Fig. 2, the projections of the system dynamics onto the $x - y, x - z$ and $y - z$ planes reveal complex, intertwined trajectories that do not converge to fixed points or closed periodic orbits. Instead, the trajectories evolve within a bounded region of the phase space, forming a structured yet non-repeating pattern. This behavior is a characteristic feature of a strange attractor.

The $x - y$ phase portrait demonstrates a butterfly-like structure with multiple loops, indicating strong nonlinear interactions between the x and y state variables. The trajectories densely fill a confined region without overlapping in a periodic manner, which suggests sensitive dependence on initial conditions. Similarly, the $x - z$ projection exhibits folded and stretched trajectories, reflecting the nonlinear coupling introduced by the xz and yz terms in Equation (1). These stretching and folding mechanisms are fundamental processes responsible for the generation of chaos.

The $y - z$ phase portrait presents a more compact but still highly intricate structure, where trajectories continuously circulate within a bounded region while maintaining irregular spacing. This indicates that although the system is dissipative, it preserves complex internal dynamics. The absence of trajectory convergence in all two-dimensional projections confirms that the system does not settle into equilibrium or periodic motion.

The three-dimensional phase portrait shown in Fig. 2 provides a comprehensive visualization of the system dynamics. The attractor exhibits a double-scroll-like structure, where trajectories orbit around two distinct regions in state space. These regions correspond to unstable equilibrium points, around which the system states continuously evolve without settling. The trajectory transitions between these regions in an irregular manner, further confirming the chaotic nature of the system.

Another important observation is that the trajectories remain confined within a finite volume in the three-dimensional state space. This boundedness is consistent with dissipative dynamics and a bounded attractor, despite the strong sensitivity to initial conditions. Such behavior is important for practical control design because it prevents unbounded state growth.

Phase portrait analysis confirms that the Newton–Leipnik system defined in Equation (1) exhibits a well-defined strange attractor under the selected parameter value $m = 5$. These results complement the time series analysis presented in the previous section and provide strong geometric evidence of chaotic behavior, forming a basis for subsequent Lyapunov exponent analysis and control design.

Lyapunov exponents

To quantitatively confirm chaotic dynamics in the Newton–Leipnik system, Lyapunov exponents are calculated. They measure the average exponential divergence or convergence of nearby trajectories in phase space. At least one positive exponent is a strong indicator of chaos when supported by the bounded aperiodic trajectories and attractor geometry reported here.

The time evolution of the Lyapunov exponents corresponding to the system defined in Equation (1) is illustrated in Figure 3. As observed in Fig. 3, the largest Lyapunov exponent λ_1 converges to a positive value after the transient phase, indicating exponential divergence of nearby trajectories. This confirms that the system exhibits sensitive dependence on initial conditions, which is a fundamental characteristic of chaotic systems.

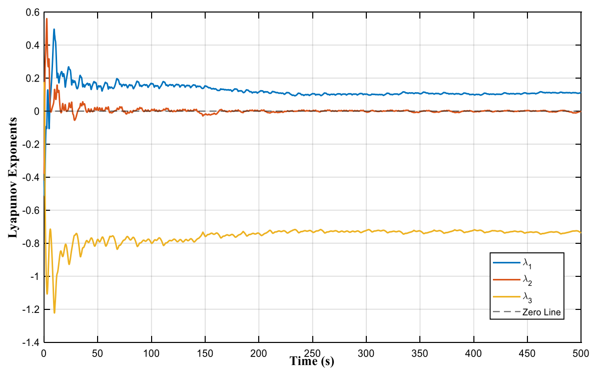

Figure 3. Lyapunov exponents of the Newton–Leipnik system.

The second Lyapunov exponent λ_2 approaches a value close to zero, suggesting that the system dynamics evolve along a neutral direction in phase space. This behavior is commonly associated with the flow direction of continuous-time dynamical systems. The third Lyapunov exponent λ_3 converges to a negative value, indicating contraction along at least one dimension of the state space.

The combination of one positive, one near-zero, and one negative Lyapunov exponent satisfies the typical signature of a dissipative chaotic system. This structure implies that while trajectories diverge in one direction, they are simultaneously compressed in others, resulting in a bounded attractor.

Another important observation from Fig. 3 is that the Lyapunov exponents initially exhibit transient fluctuations before converging to steady values. This transient phase corresponds to the system's adjustment from the initial conditions toward the attractor. After this phase, the exponents stabilize, providing reliable estimates of the system's long-term dynamical behavior. Furthermore, the sum of the Lyapunov exponents is negative, indicating that the system is dissipative. This implies that the volume in phase space contracts over time, leading to the formation of a strange attractor. The dissipative nature of the system is consistent with the bounded trajectories observed in both the time series (Fig. 1) and phase portraits (Fig. 2).

Lyapunov exponent analysis provides strong quantitative evidence that the Newton–Leipnik system, under the selected parameter value $m = 5$, operates in a chaotic regime. These results complement the qualitative observations obtained from time series and phase portrait analyses, and they establish a solid foundation for the subsequent bifurcation analysis and control design.

The largest Lyapunov exponent, $\lambda_1 = 0.125358$, is positive, which indicates exponential divergence of nearby trajectories and confirms the sensitive dependence on initial conditions. The second exponent, $\lambda_2 = 0.001085$, is very close to zero, which is a typical property of continuous-time dynamical systems and is generally associated with the flow direction of the trajectory. The third exponent, $\lambda_3 = -0.751443$, is negative, indicating contraction along at least one dimension of the phase space. The coexistence of one positive, one near-zero, and one negative Lyapunov exponent confirms that the Newton–Leipnik system exhibits dissipative chaotic behavior. In addition, the sum of the Lyapunov exponents $\lambda_1 + \lambda_2 + \lambda_3$ is -0.625000, which means that the system is dissipative, so that phase-space volumes contract over time. This contraction is consistent with the bounded attractor structure observed in the phase portraits.

To further characterize the fractal nature of the attractor, the Kaplan–Yorke dimension was calculated. The Kaplan–Yorke dimension is given by Equation (3)

$$D_{KY} = j + \frac{\sum_{i=1}^{j} \lambda_i}{|\lambda_{j+1}|} \tag{3}$$

where j is the largest integer satisfying Equation (4)

$$\sum_{i=1}^{j} \lambda_i \geq 0 \tag{4}$$

For the present system, since $\lambda_1 + \lambda_2 = 0.126443 > 0$ and $\lambda_1 + \lambda_2 + \lambda_3 < 0$, the value of j is obtained as $j = 2$. Accordingly, the Kaplan–Yorke dimension is found as $D_{KY} = 2.168267$.

The non-integer value of the Kaplan–Yorke dimension indicates that the attractor has a fractal structure with a dimension between 2 and 3, which is a typical characteristic of strange attractors in chaotic dynamical systems. Therefore, the Lyapunov exponent spectrum, the negative sum of exponents, and the Kaplan–Yorke dimension collectively provide strong quantitative evidence that the Newton–Leipnik system operates in a fully developed chaotic regime for m=5.

Bifurcation analysis

To further investigate the effect of the system parameter m on the dynamical behavior of the Newton–Leipnik system, bifurcation analysis is performed. Bifurcation diagrams provide a global view of how the qualitative structure of system trajectories changes as a control parameter varies. In this study, the parameter m in Equation (1) is selected as the bifurcation parameter, and its influence on the system dynamics is examined over a specified range.

The bifurcation diagram corresponding to the z-state variable is presented in Figure 4. In this diagram, the local maxima of z_t are plotted against the varying parameter m, allowing the identification of transitions between periodic and chaotic regimes.

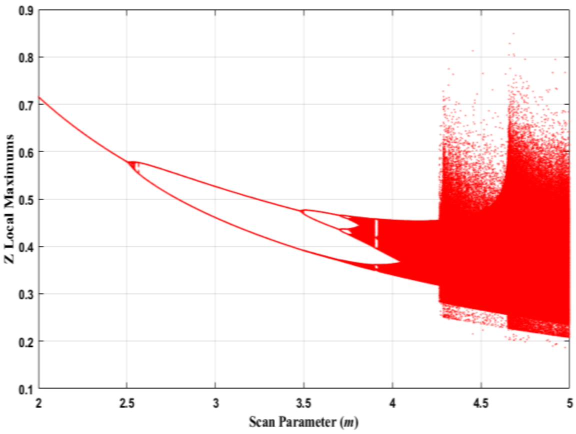

Figure 4. Bifurcation diagram of the Newton–Leipnik system with respect to parameter m.

As shown in Fig. 4, the system initially exhibits a single-valued response for lower values of m, indicating stable or periodic behavior. As the parameter increases, the system undergoes a sequence of bifurcations, where the number of distinct solution branches increases. This behavior is characteristic of a period-doubling route to chaos, where the system transitions from a stable periodic orbit to increasingly complex oscillatory patterns.

In the intermediate parameter range ($m \approx 3.5 - 4.2$), the system displays multiple branches, indicating higher-period oscillations and the onset of instability. As m increases further, the bifurcation diagram becomes densely populated, forming a continuous band of points. This region corresponds to fully developed chaotic behavior, where the system no longer exhibits periodicity and instead evolves in an aperiodic and unpredictable manner.

Another important observation from Fig. 4 is the presence of irregular structures within the chaotic region, suggesting the existence of periodic windows embedded within chaos. These windows represent parameter intervals where the system temporarily regains periodic behavior before returning to chaotic dynamics. Such behavior is a well-known feature of nonlinear dynamical systems and further confirms the complex nature of the Newton–Leipnik system.

The results of the bifurcation analysis are consistent with the time series (Fig. 1), phase portraits (Fig. 2), and Lyapunov exponent results (Fig. 3). In particular, the parameter value $m = 5$, selected for detailed analysis in this study, clearly lies within the chaotic region of the bifurcation diagram. This validates the choice of operating point for subsequent control design.

Overall, the bifurcation diagram provides strong evidence of the rich nonlinear dynamics exhibited by the Newton–Leipnik system and highlights the critical role of the parameter m in governing system behavior. These findings establish a comprehensive understanding of the system dynamics and form a crucial basis for the design of robust control strategies in the following sections.

Sliding mode control design

Sliding Mode Control (SMC) is a robust nonlinear control technique widely used for systems with uncertainties, nonlinearities, and external disturbances. The main principle of SMC is to force the system trajectories onto a predefined sliding surface and maintain them on this surface despite disturbances. Once the system reaches the sliding surface, the dynamics become insensitive to parameter variations and external perturbations, making SMC particularly suitable for chaotic systems. In this study, the SMC approach is applied to the Newton–Leipnik chaotic system given in Equation (1) to suppress chaotic oscillations and stabilize the system at the equilibrium point. The control objective is defined as $x_{ref} = y_{ref} = z_{ref} = 0$. Accordingly, the controlled form of the system is expressed by augmenting Equation (1) with control inputs and disturbance terms, as shown in Equation (5):

$$\begin{aligned} \dot{x} &= -0.4x + y + 10yz + u_1 + d_x \\ \dot{y} &= -x - 0.4y + mxz + u_2 + d_y \\ \dot{z} &= 0.175z - 5xy + u_3 + d_z \end{aligned} \tag{5}$$

Since the reference values are zero, the tracking errors directly correspond to the system states. Based on this, the sliding surfaces are defined as given in Equation (6):

$$s_1 = x, \qquad s_2 = y, \qquad s_3 = z \tag{6}$$

The control law is designed by combining nonlinear dynamics compensation with a constant-plus-proportional-rate reaching law [29], as presented in Equation (7):

$$u_i = -f_i(x, y, z) - \lambda_i s_i - k_i sat\left(\frac{s_i}{\Phi_i}\right) \qquad (7)$$

where $f_i(x, y, z)$ denotes the right-hand side of the system dynamics given in Equation (1), which is cancelled exactly by the first control term, $k_i > 0$ are the switching gains, $\lambda_i > 0$ are the proportional reaching gains, and $\Phi_i > 0$ are the boundary-layer thicknesses. The first term cancels the system dynamics exactly, the second term imposes a proportional rate of convergence toward the sliding surface, and the third term provides robustness against bounded disturbances. The resulting structure corresponds to a constant-plus-proportional-rate reaching law, in which the reaching speed is governed by λ_i and the disturbance rejection capability by k_i.

In Equation (7), the term $\mathrm{sat}(s_i/\Phi_i)$ denotes the saturation function with boundary layer Φ_i, defined as $\mathrm{sat}(\sigma) = \sigma$ for $|\sigma| \leq 1$ and $\mathrm{sat}(\sigma) = \mathrm{sign}(\sigma)$ otherwise. Outside the boundary layer, that is, for $|s_i| > \Phi_i$, the saturation function reduces to the discontinuous sign function, so the control action always acts in the direction opposite to the sliding variable and drives the trajectory toward $s_i = 0$ in finite time. Inside the boundary layer, $|s_i| \leq \Phi_i$, the discontinuous switching is replaced by a high-gain linear feedback of slope k_i/Φ_i, so that the control signal remains continuous. This continuity is the mechanism by which the boundary layer suppresses chattering; the price paid is that asymptotic convergence to the origin is replaced by convergence to a small residual set, the size of which is quantified in Equation (13). All simulations reported in this paper employ the saturation function with $\Phi_1 = \Phi_2 = \Phi_3 = 0.02$. The discontinuous sign function is used only in the comparative study of switching functions presented in Figure 10 and Table 4.

The control gain k_i determines the magnitude of the switching control action. Its value must be selected sufficiently large to dominate the effects of model uncertainties and external disturbances. In general, if the disturbance acting on the $i\text{-}th$ state is bounded by $|d_i| \leq d_{imax}$, the gain should satisfy $k_i > d_{imax}$ so that the reaching condition $s_i * \dot{s}_i < 0$ is maintained. This condition guarantees that the system trajectory moves toward the sliding surface rather than diverging from it. However, selecting k_i excessively large may produce high-frequency oscillations in the control signal, known as chattering, and may also increase the required control effort. Therefore, k_i should be chosen by considering a balance between fast convergence, disturbance rejection capability, and smooth control action.

In this study, the gains k_1, k_2 and k_3 are selected through simulation-based tuning. First, the gains are chosen high enough to suppress the chaotic oscillations of the uncontrolled Newton–Leipnik system. Then, they are gradually adjusted to obtain rapid convergence after controller activation while avoiding excessive control fluctuations. The final selected gain values provide a stable response, bounded control inputs, and effective disturbance rejection under both impulsive and sinusoidal disturbance conditions. As observed from the simulation results, the selected gains allow the system states to converge rapidly to the reference value after SMC activation and maintain stability even when external disturbances are introduced. The final values adopted throughout this study are $\lambda_1 = \lambda_2 = \lambda_3 = 3$, $k_1 = k_2 = k_3 = 6$ and $\Phi_1 = \Phi_2 = \Phi_3 = 0.02$. Since the disturbance amplitude is bounded by $\overline{d}_i = 0.5$, the reaching condition $k_i > \overline{d}_i$ is satisfied with a margin of a factor of twelve. All design and simulation parameters are summarised in Table 1.

Table 1. Design and simulation parameters of the Newton–Leipnik system and the proposed sliding mode controller.

Parameter	Symbol	Value
System parameter	m	5
Initial condition	x_0	(0.349, 0, −0.16)
Reference (set point)	x_r	(0, 0, 0)
Simulation horizon	t_f	100 s
Controller activation time	t_{SMC}	45 s
Proportional reaching gains	$\lambda_1, \lambda_2, \lambda_3$	3, 3, 3
Switching gains	k_1, k_2, k_3	6, 6, 6
Boundary-layer thicknesses	Φ_1, Φ_2, Φ_3	0.02, 0.02, 0.02
Gaussian impulse centre	t_{imp}	70 s
Gaussian impulse width	σ_{imp}	0.08 s
Gaussian impulse amplitude	d_{imp}	$[0.5, -0.5, 0.5]^{\mathrm{T}}$
Sinusoidal disturbance interval	–	75 − 80 s
Sinusoidal disturbance amplitude	d_{sin}	$[0.5, -0.5, 0.5]^{\mathrm{T}}$
Sinusoidal disturbance frequency	f_{sin}	1 Hz
Disturbance bound	$\overline{d}_i$	0.5
Numerical solver	–	ode45 (RelTol = 10^{-7}, AbsTol = 10^{-9})

To analyze the stability of the closed-loop system, a Lyapunov function is selected as given in Equation (8):

$$V = \frac{1}{2}(x^2 + y^2 + z^2) \qquad (8)$$

Since the reference is the origin, the sliding variables coincide with the system states, $s = [x\, y\, z]^{\mathrm{T}}$, so that the function in Equation (8) is positive definite and radially unbounded. Substituting the control law of Equation (7) into the disturbed system of Equation (5) cancels f_i exactly and decouples the three error channels, which yields the closed-loop sliding dynamics given in Equation (9):

$$\dot{s}_i = -\lambda_i s_i - k_i sat\left(\frac{s_i}{\Phi_i}\right) + d_i \qquad (9)$$

The time derivative of V along the trajectories of Equation (9) is then obtained as given in Equation (10):

$$\dot{V} = \sum_{i=1}^{3} s_i \dot{s}_i = -\sum_{i=1}^{3} \lambda_i {s_i}^2 - \sum_{i=1}^{3} k_i s_i sat\left(\frac{s_i}{\Phi_i}\right) + \sum_{i=1}^{3} s_i d_i \tag{10}$$

Case 1: disturbance-free system. For $d_i = 0$, Equation (10) reduces to Equation (11):

$$\dot{V} = -\sum_{i=1}^{3} \lambda_i {s_i}^2 - \sum_{i=1}^{3} k_i s_i sat\left(\frac{s_i}{\Phi_i}\right) \leq -\sum_{i=1}^{3} \lambda_i {s_i}^2 < 0 \tag{11}$$

The product $s_i\ \mathrm{sat}(s_i/\Phi_i)$ is non-negative for every s_i and is strictly positive for $s_i \neq 0$; hence, the inequality in Equation (11) is strict and $\dot{V}$ is negative definite. The origin of the disturbance-free closed loop is therefore asymptotically stable in the sense of Lyapunov. Moreover, inside the boundary layer, the sliding dynamics reduce to the linear form $\dot{s}_i = -(\lambda_i + k_i/\Phi_i)s_i$, so convergence is exponential with the time constant $1/(\lambda_i + k_i/\Phi_i) =$ 3.3 ms for the gains adopted here. This first-order structure also explains why no overshoot is observed in any state channel in Table 2.

Case 2: system subject to bounded disturbances. Let the disturbance acting on the i-th state be bounded by $|d_i| \leq \bar{d}_i$. Outside the boundary layer, that is, for $|s_i| > \Phi_i$, the saturation function satisfies $\mathrm{sat}(s_i/\Phi_i) = \mathrm{sign}(s_i)$, and therefore $s_i\ \mathrm{sat}(s_i/\Phi_i) = |s_i|$. Applying the bound $s_i d_i \leq |s_i|\bar{d}_i$ to the last term of Equation (10) gives Equation (12):

$$\dot{V} \leq -\sum_{i=1}^{3} \lambda_i {s_i}^2 - \sum_{i=1}^{3} (k_i - \bar{d}_i)|s_i| < 0 \tag{12}$$

Consequently, $\dot{V} < 0$ holds for every state outside the boundary layer provided that the gain condition $k_i > \bar{d}_i$ is satisfied. In the present study, $\bar{d}_i = 0.5$ and $k_i = 6$, so the condition holds with a margin of a factor of twelve, and the trajectories reach the boundary layer in finite time. Inside the boundary layer, the closed loop becomes $\dot{s}_i = -(\lambda_i + k_i/\Phi_i)s_i + d_i$, which is a stable first-order system driven by a bounded input. Its solution is therefore uniformly ultimately bounded, and the ultimate bound follows directly as given in Equation (13):

$$|s_i| \leq \frac{\bar{d}_i}{\lambda_i + \dfrac{k_i}{\Phi_i}} \tag{13}$$

For $\lambda_i = 3, k_i = 6, \Phi_i = 0.02$, and $\bar{d}_i = 0.5$, Equation (13) predicts $|s_i| \leq 1.6502 \times 10^{-3}$. The largest absolute state deviation observed in the simulations is 1.6488×10^{-3} under the Gaussian impulse and 1.6498×10^{-3} under the sinusoidal disturbance, so the analytical bound and the numerical results agree to four significant digits. It should be emphasised that, because a boundary layer is used, the disturbed closed loop is uniformly ultimately bounded rather than asymptotically stable; the residual set can be made arbitrarily small by reducing Φ_i, at the cost of increased switching activity, as quantified in Table 4.

Before applying the control strategy, the uncontrolled response of the Newton–Leipnik system is analyzed to clearly demonstrate its inherent chaotic behavior. As shown in Figure 5, the system exhibits irregular, non-periodic, and high-amplitude oscillations in all state variables. These oscillations persist over time without any convergence, confirming the chaotic nature of the system as previously discussed through time series, phase portraits, and Lyapunov exponent analyses.

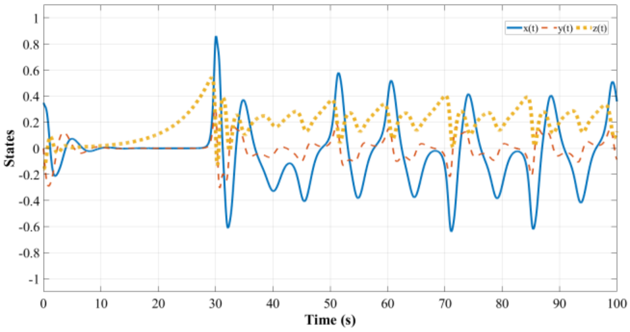

Figure 5. Uncontrolled time response of the Newton–Leipnik system.

To suppress this chaotic behavior, the sliding mode controller defined in Equation (7) is activated at approximately $t = 45$s. This intentional delay allows a direct comparison between the uncontrolled and controlled dynamics. The system response before and after controller activation is illustrated in Figure 6.

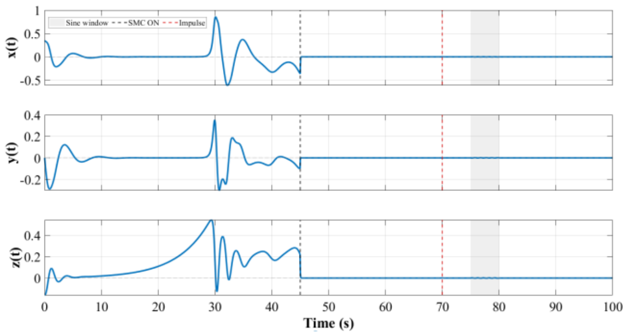

Figure 6. Time responses of the x(t), y(t) and z(t) states before and after SMC activation.

As observed, once the controller is engaged, all state variables rapidly converge to the equilibrium point. The chaotic oscillations are completely eliminated, and the system transitions into a stable regime within a short time interval. This result clearly demonstrates the effectiveness of the proposed SMC strategy. The corresponding, the transient performance measures extracted from the simulation are reported in Table 2. The 2 % settling times are 0.056 s, 0.020 s and 0.036 s for x, y and z respectively, no overshoot occurs in any state channel, and the peak control magnitudes remain bounded by 7.26. The absence of overshoot is a direct consequence of the first-order error dynamics inside the boundary layer, as shown in Case 1 of the stability analysis.

Table 2. Transient performance of the closed-loop system after controller activation at $t = 45$ s, evaluated over the nominal disturbance-free interval 45–68 s. t_s is the 2 % settling time measured from activation, OS the overshoot, and e_{ss} the steady-state error.

State	Value at $t = 45$ s	t_s (2%)	OS [%]	$\lvert e_{ss}\rvert$	$\max\lvert u_i\rvert$
x	−0.3630	0.0555	0.00	$< 10^{-12}$	7.259
y	−0.0993	0.0200	0.00	$< 10^{-12}$	6.289
z	0.2169	0.0360	0.00	$< 10^{-12}$	6.508

To further evaluate the robustness of the controller, external disturbances are introduced into the system. The disturbance profiles are presented in Figure 7.

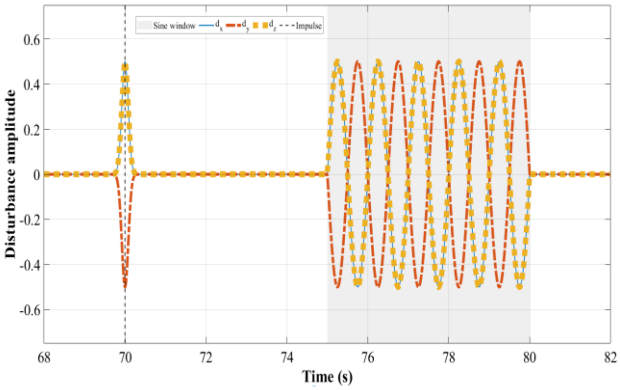

Figure 7. Applied Gaussian impulse and sinusoidal disturbance signals.

Two different types of disturbances are considered: a Gaussian impulse and a sinusoidal disturbance. The Gaussian impulse represents sudden and high-energy perturbations such as shocks or abrupt system variations, while the sinusoidal disturbance represents continuous oscillatory effects such as vibrations and environmental disturbances. Both disturbances are injected directly into the three state equations of Equation (5) with the amplitude vectors $d_{imp} = d_{sin} = [0.5, -0.5, 0.5]^{\mathrm{T}}$. The Gaussian impulse is centred at t = 70 s with a standard deviation of 0.08 s, and the sinusoidal disturbance has a frequency of 1 Hz and acts over the interval t = 75–80 s. The two events do not overlap in time, so the disturbance acting on each state is bounded by $\overline{d_i} = 0.5$, which is the value used in the gain condition of the stability analysis.

The applied disturbance signals, including both Gaussian impulse and sinusoidal disturbances, are presented in Figure 7. The corresponding system responses under these disturbances are illustrated in Figure 8. As observed, the Gaussian impulse causes a temporary deviation of the state variables from the equilibrium point. However, the controller rapidly compensates for this effect and drives the system back to the reference value within a short time interval. This behavior demonstrates strong robustness against sudden disturbances.

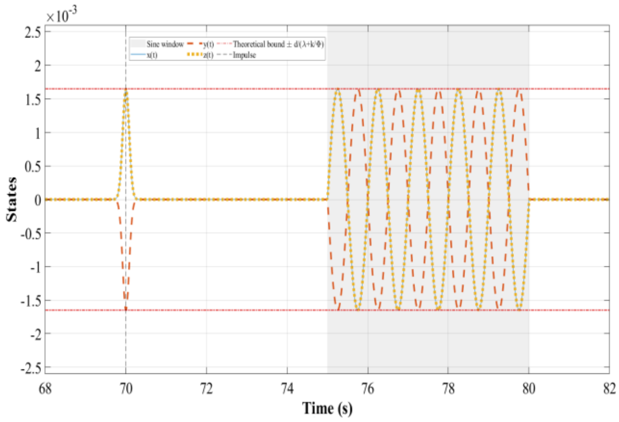

Figure 8. System response under Gaussian impulse and sinusoidal disturbances.

In the case of the sinusoidal disturbance, the system remains stable and exhibits only small-amplitude oscillations around zero. These oscillations are bounded and do not increase over time, indicating that the controller effectively rejects persistent disturbances. The overall response confirms that the proposed SMC strategy maintains stability and robustness under both impulsive and continuous disturbance conditions. Figure 8 additionally shows the theoretical ultimate bound of $\pm 1.6502 \times 10^{-3}$ predicted by Equation (13). The state trajectories remain inside this band throughout both disturbance events, which provides a direct numerical confirmation of the stability analysis. The corresponding error indices are reported in Table 3. It should be noted that the indices of the three states are identical in the disturbed intervals. This follows from the structure of the closed loop: the control law of Equation (7) cancels the coupling terms exactly, so the three error channels become decoupled and identical in structure, and since the disturbance amplitudes have equal magnitude on all three states, the error of y differs from that of x and z only by its sign.

The control input u_3, depicted in Figure 9, provides further insight into the controller performance. The control signal remains close to zero after stabilisation and becomes active only during the disturbance intervals. During the impulsive disturbance the control input exhibits a sharp transient response, whereas during the sinusoidal disturbance it oscillates adaptively in order to counteract the external excitation. This indicates that the controller operates efficiently and applies control effort only when it is necessary. In order to resolve the switching behaviour of the control signal, Figure 9 also includes two magnified views on a 0.4 s time scale, taken immediately after controller activation and within the sinusoidal disturbance interval. In both windows the control signal is continuous and free of high-frequency switching, which confirms that the boundary layer introduced in Equation (7) suppresses chattering. The behaviour that would be obtained with the discontinuous sign function is examined in the following subsection.

Table 3. Error performance indices of the closed-loop system. Nominal interval 45–68 s, Gaussian impulse interval 69–74 s, sinusoidal disturbance interval 75–81 s. The tracking error equals the state because the reference is the origin. In the two disturbed intervals the three channels give identical index values, because the control law decouples them and the disturbance amplitudes have equal magnitude on all three states.

Index	Nominal x	Nominal y	Nominal z	Impulse $x/y/z$	Sine $x/y/z$
ISE	$2.34e^{-3}$	$5.27e^{-5}$	$5.25e^{-4}$	$3.86e^{-7}$	$6.80e^{-6}$
IAE	$9.84e^{-3}$	$8.29e^{-4}$	$3.69e^{-3}$	$3.31e^{-4}$	$5.25e^{-3}$
ITAE	$1.81e^{-4}$	$4.87e^{-6}$	$4.27e^{-5}$	$3.32e^{-4}$	$1.31e^{-2}$
RMSE	$1.02e^{-2}$	$1.55e^{-3}$	$4.83e^{-3}$	$2.78e^{-4}$	$1.06e^{-3}$
$\lvert e\rvert_{\max}$	$3.63e^{-1}$	$9.93e^{-2}$	$2.17e^{-1}$	$1.65e^{-3}$	$1.65e^{-3}$

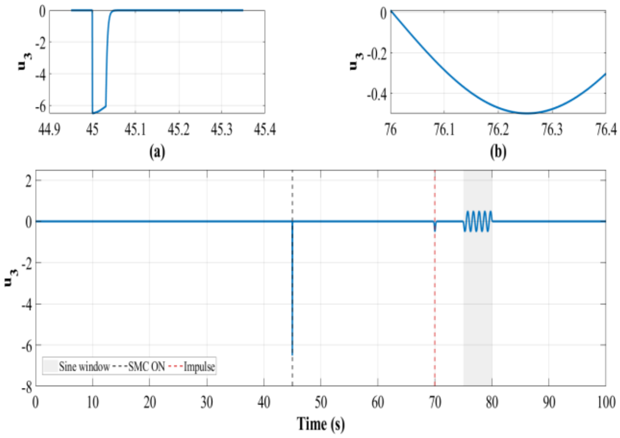

Figure 9. Control input u_3 with two magnified views resolving the control signal after controller activation (a) and within the sinusoidal disturbance interval (b). The signal is continuous in both windows, which shows that the boundary layer eliminates chattering.

Chattering analysis and choice of the switching function

Because the sign function is discontinuous, it forces the control signal to switch at the highest frequency the actuator or the numerical solver permits, which produces the well-known chattering phenomenon. Chattering excites unmodelled high-frequency dynamics and increases actuator wear, so its severity is quantified in this subsection. Two families of remedies are common in the literature: continuous approximation of the sign function, and higher-order sliding mode design. The present work adopts the first approach through the boundary-layer saturation function already introduced in Equation (7).

A natural question is whether an alternative smooth function, such as the hyperbolic sine, could be used instead. The hyperbolic sine is not a suitable candidate for two reasons. First, $\sinh(\sigma)$ is unbounded and grows exponentially with $|\sigma|$, so the switching term would generate arbitrarily large control amplitudes whenever the state is far from the sliding surface. This would drive the actuator into saturation and would also invalidate the bound used in Equation (12). Second, its slope at the origin is unity, whereas chattering reduction requires a steep but finite slope in a thin layer around the sliding surface. An admissible replacement for $\operatorname{sign}(\sigma)$ must therefore be bounded, monotonic, odd, and must approach ± 1 for $|\sigma| \gg 0$. The saturation function $\operatorname{sat}(\sigma)$ and the hyperbolic tangent $\tanh(\sigma)$ satisfy these requirements; $\sinh(\sigma)$ does not.

To quantify the effect of the switching function, the closed-loop system was simulated with the three alternatives $\operatorname{sign}(s_i)$, $\operatorname{sat}(s_i/\Phi_i)$, and $\tanh(s_i/\Phi_i)$, while all remaining gains were kept fixed at the values in Table 1. To ensure a fair comparison, all three cases were integrated with the same fixed-step fourth-order Runge–Kutta scheme with a step size of 10^{-4} s, because adaptive-step solvers artificially smooth the switching of the sign function and therefore mask chattering. The severity of chattering is measured by the total variation of the control signal after controller activation, $\mathrm{TV}(u_3) = \sum_k |u_3(k+1) - u_3(k)|$, which increases with the amount of switching. The results are shown in Figure 10 and summarised in Table 4.

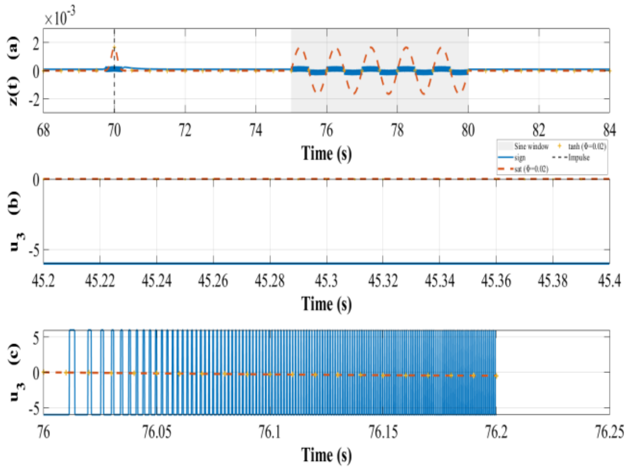

Figure 10. Comparison of the switching functions: (a) state response $z(t)$ under the disturbances, (b) magnified control signal immediately after controller activation, (c) magnified control signal within the sinusoidal disturbance interval. Chattering is visible only for the sign function.

With the discontinuous sign function, the control signal switches continuously between its extreme values, giving $\mathrm{TV}(u_3) = 1.0141 \times 10^5$ and a root-mean-square control effort of 6.00, which means that the actuator is fully engaged at all times. The boundary-layer saturation function reduces the total variation to 17.51, that is, by a factor of approximately 5.8×10^3, and reduces the root-mean-square control effort by a factor of 31.7. The hyperbolic tangent yields essentially identical figures, which is expected because the two functions differ appreciably only within the boundary layer. The price of this reduction is an increase of the ultimate error bound by a factor of five, from 3.25×10^{-4} with the sign function to 1.65×10^{-3} with the saturation function, which remains negligible for the present application. This trade-off, together with the practical requirement of a continuous control signal, is the reason why the saturation function is used throughout this study.

Table 4. Effect of the switching function on chattering, control effort, and steady-state accuracy ($t > 45$ s, identical gains, fixed-step RK4 with $h = 10^{-4}$ s, $\Phi_i = 0.02$). TV denotes the total variation of the control signal, used here as the quantitative measure of chattering.

$g(s_i)$	RMSE u_3	TV u_3	IAE z	max$\|z\|$ (sine)
$\mathrm{sign}(s_i)$	$6.00e^{+0}$	$1.01e^{+5}$	$9.38e^{-3}$	$3.25e^{-4}$
$\mathrm{sat}(s_i/\Phi_i)$	$1.89e^{-1}$	$1.75e^{+1}$	$9.27e^{-3}$	$1.65e^{-3}$
$\tanh(s_i/\Phi_i)$	$1.88e^{-1}$	$1.75e^{+1}$	$9.30e^{-3}$	$1.65e^{-3}$

Results and discussion

The uncontrolled Newton–Leipnik system was first examined to verify whether the selected operating condition, m=5, leads to a chaotic regime. The obtained state responses exhibited sustained irregular oscillations without convergence to an equilibrium point or periodic orbit. Although the trajectories remained bounded, their temporal evolution was clearly aperiodic, indicating that the system operates in a highly nonlinear and complex regime.

The phase-space behavior supported this observation by revealing a bounded but non-repeating attractor structure. Rather than collapsing to a fixed point or a limit cycle, the trajectories evolved within a confined region of the state space, forming a characteristic strange attractor. In addition, the Lyapunov exponent analysis confirmed the chaotic regime quantitatively through the presence of a positive largest Lyapunov exponent, indicating exponential divergence of neighboring trajectories. The bifurcation analysis further showed that the parameter m strongly affects the global dynamics of the system and that the selected operating point m=5 lies within a chaotic region.

After verifying the uncontrolled chaotic behavior, the proposed sliding mode controller was applied to regulate all state variables to the origin. Before controller activation, the states maintained irregular chaotic oscillations. The controller was intentionally activated at approximately t=45 s in order to distinguish the uncontrolled and controlled regimes within the same simulation interval. Once the controller was engaged, the state trajectories rapidly converged toward zero and the chaotic oscillations were effectively suppressed. This result demonstrated that the proposed control law successfully stabilized the Newton–Leipnik system.

To evaluate robustness, two different external disturbances were introduced after the system had been stabilized. A Gaussian impulse disturbance was applied at t=70 s, while a sinusoidal disturbance was imposed over the interval of t=75–80 s. Under the Gaussian impulse, the state variables exhibited a brief deviation from the equilibrium point; however, the controller quickly compensated for this perturbation and restored the system to the desired reference within a short time. During the sinusoidal disturbance interval, the state variables remained close to zero and displayed only small-amplitude bounded oscillations. These oscillations did not grow over time and did not reintroduce chaotic motion.

The control inputs also remained bounded throughout the simulation. Strong control activity appeared mainly during controller activation and disturbance intervals. During the initial stabilization stage, transient peaks were observed in the control signals as the controller suppressed the pre-existing chaotic oscillations. After stabilization, the control effort decreased significantly. When the Gaussian impulse was applied at t=70 s, the control inputs generated sharp corrective responses. During the sinusoidal disturbance interval of t=75–80 s, the control signals oscillated adaptively to compensate for the external excitation. Overall, the obtained results showed that the proposed sliding mode controller achieved rapid stabilization, effective disturbance rejection, and bounded control effort.

The obtained results are consistent with the general theory of deterministic chaos reported in the literature. Irregular but bounded oscillations, strange attractor formation, positive Lyapunov exponents, and parameter-dependent bifurcation behavior are all recognized as fundamental characteristics of chaotic systems [1–4]. In this respect, the present findings confirm that the Newton–Leipnik system belongs to the class of nonlinear dissipative systems whose long-term behavior cannot be described by equilibrium-based or purely periodic interpretations. Moreover, the use of multiple diagnostic tools in this study is important because previous studies have emphasized that chaos identification should not rely on a single indicator alone, but should instead be supported by complementary temporal, geometric, and stability-based evidence [3,6].

The bifurcation analysis also agrees with the broader nonlinear dynamics literature, where parameter variation is known to induce qualitative transitions in system behavior [2–4]. In the present study, the parameter m clearly acts as a bifurcation parameter controlling the transition from more regular oscillatory responses to chaotic motion. The fact that m=5 is located inside a chaotic region indicates that the control problem considered here is nontrivial and corresponds to a fully developed chaotic regime rather than a weakly perturbed oscillatory state.

From the control perspective, the results confirm the suitability of sliding mode control for chaotic nonlinear systems. SMC is widely recognized as an effective robust control strategy for systems with uncertainties, nonlinearities, and bounded disturbances because of its reaching property and insensitivity to perturbations on the sliding manifold [18,22,30]. The rapid suppression of chaotic oscillations observed in this study is consistent with previous reports on Lorenz-type chaotic systems and other nonlinear models stabilized using sliding-mode-based approaches [18,22,30]. Similarly, the strong disturbance rejection performance obtained here agrees with the broader literature showing that robust nonlinear controllers can maintain stability in chaotic systems even in the presence of external perturbations [19–21].

An important contribution of the present study is the explicit evaluation of robustness under two fundamentally different disturbance classes. The Gaussian impulse applied at t=70 s tested the transient disturbance-rejection capability of the controller against a sudden high-intensity perturbation, whereas the sinusoidal disturbance imposed over t=75–80 s assessed closed-loop performance under persistent oscillatory excitation. The successful rejection of both signals demonstrates that the controller is not limited to nominal stabilization, but is also capable of preserving regulation under more realistic disturbance scenarios. This is particularly important for chaotic systems, whose sensitivity to perturbations can easily amplify small deviations if the controller is not sufficiently robust.

The bounded nature of the control inputs is also significant in practical terms. Although sliding mode control is known for its robustness, excessively high gain values may lead to unnecessarily aggressive switching behavior and increased actuation demand. In the present work, the control gains were selected by considering the trade-off between convergence speed, robustness, and bounded control effort. The resulting responses indicate that the adopted gain set provides an effective compromise: the system converges rapidly, rejects both impulsive and oscillatory disturbances, and does so without requiring excessive sustained control action.

The present findings also fit within the broader engineering perspective of chaos-related studies. Previous works have shown that chaotic dynamics can be exploited advantageously in practical systems such as magnetic stirring, robotic end-effector control, and biogas mixing applications [15–17]. In contrast, the current study addresses the complementary problem of suppressing undesirable chaotic oscillations in order to obtain stable regulation. Taken together, these studies highlight the dual role of chaos in engineering systems: it may either be exploited as a beneficial mechanism or controlled as an unwanted source of instability, depending on the application objective.

Overall, the discussion indicates that the Newton–Leipnik system provides a meaningful benchmark for robust chaos-control studies and that the proposed sliding mode control strategy offers a reliable method for stabilizing such dynamics. The agreement between the present findings and the existing literature supports the validity of the results and demonstrates the broader relevance of the proposed approach within nonlinear control research.

Conclusion

This study presented the mathematical formulation, dynamical analysis, and sliding mode control of the Newton–Leipnik chaotic system. The system was first analyzed in its uncontrolled form to determine its nonlinear characteristics under the selected operating condition. Time responses, phase portraits, Lyapunov exponents, and bifurcation analysis consistently confirmed that the Newton–Leipnik system exhibits fully developed chaotic behavior for m=5. The results demonstrated that the system possesses bounded but aperiodic trajectories, a strange attractor structure, a positive largest Lyapunov exponent, and parameter-dependent transitions to chaos.

The proposed controller, activated at t = 45 s, suppressed the chaotic oscillations with 2 % settling times below 0.06 s and without overshoot in any state channel. Under a Gaussian impulse at t = 70 s and a sinusoidal disturbance over t = 75–80 s, the state deviations remained within 1.65×10^{-3}, in agreement with the ultimate bound derived analytically in Equation (13), and the associated RMSE values were 2.78×10^{-4} and 1.06×10^{-3} respectively. The comparison of switching functions showed that the boundary layer reduces the total variation of the control signal by more than three orders of magnitude with respect to the discontinuous sign function, at the cost of a fivefold increase in the residual error bound.

Overall, the findings of this study demonstrate that sliding mode control is a reliable and effective approach for the robust stabilization of the Newton–Leipnik chaotic system. The proposed framework not only suppresses chaotic behavior under nominal conditions but also maintains stable performance under impulsive and oscillatory disturbances. Therefore, the Newton–Leipnik system can serve as a meaningful benchmark for future studies on chaos suppression, robust nonlinear control, and disturbance-tolerant control design.

In future work, the proposed control strategy may be extended to adaptive, fractional-order, observer-based, or terminal sliding mode control structures. In addition, experimental implementation and real-time applications on embedded control platforms may further demonstrate the practical applicability of the proposed approach in engineering systems.

Data availability statement

The data that support the findings of this study are available from the corresponding author upon reasonable request.

Ethics committee approval and conflict of interest statement

Ethics committee approval was not required for this study. The authors declare that they have no known competing financial interests or personal relationships that could have appeared to influence the work reported in this paper.

Authors' Contributions

Demirsoy MS: Study conception and design; visualization; data analysis and interpretation; drafting of the manuscript.

Hamida El Naser Y: Supervision; critical revision of the manuscript.

Funding statement

No funding was received for this manuscript.

References

[1] G. Boeing, "Visual analysis of nonlinear dynamical systems: chaos, fractals, self-similarity and the limits of prediction," *Systems*, vol. 4, no. 4, p. 37, 2016.

[2] P. B. Persson and C. D. Wagner, "General principles of chaotic dynamics," *Cardiovascular Research*, vol. 31, no. 3, pp. 332–341, 1996.

[3] X. Zeng, R. A. Pielke, and R. Eykholt, "Chaos theory and its applications to the atmosphere," *Bulletin of the American Meteorological Society*, vol. 74, no. 4, pp. 631–644, 1993.

[4] R. I. Sujith and S. A. Pawar, "An introduction to dynamical systems theory," in *Thermoacoustic Instability: A Complex Systems Perspective*. Cham, Switzerland: Springer, 2021, pp. 31–85.

[5] C. Letellier *et al*., "Some elements for a history of the dynamical systems theory," *Chaos: An Interdisciplinary Journal of Nonlinear Science*, vol. 31, no. 5, 2021.

[6] N. A. Magnitskii, "Bifurcation theory of dynamical chaos," *Chaos Theory*, vol. 11, pp. 197–215, 2018.

[7] A. Robledo, "Generalized statistical mechanics at the onset of chaos," *Entropy*, vol. 15, no. 12, pp. 5178–5222, 2013.

[8] F. Baldovin and A. Robledo, "Universal renormalization-group dynamics at the onset of chaos in logistic maps and nonextensive statistical mechanics," *Physical Review E*, vol. 66, no. 4, p. 045104, 2002.

[9] B. Luque, L. Lacasa, F. J. Ballesteros, and A. Robledo, "Feigenbaum graphs: a complex network perspective of chaos," *PLoS ONE*, vol. 6, no. 9, p. e22411, 2011.

[10] A. D. Morozov, *Invariant Sets for Windows*, vol. 37. Singapore: World Scientific, 1999.

[11] S. P. Kuznetsov, "A variety of critical phenomena associated with the golden mean quasiperiodicity," *Izvestiya VUZ. Applied Nonlinear Dynamics*, vol. 10, no. 3, p. 22, 2002.

[12] S. Banerjee and G. C. Verghese, *Nonlinear Phenomena in Power Electronics*. Piscataway, NJ, USA: IEEE Press, 1999.

[13] A. Uthamacumaran, "A review of dynamical systems approaches for the detection of chaotic attractors in cancer networks," *Patterns*, vol. 2, no. 4, 2021.

[14] V. E. Orel, S. I. Korovin, J. Molnár, and V. B. Orel, "Non-linear dynamics theory and malignant melanoma," *Experimental Oncology*, vol. 41, no. 4, pp. 291–299, 2019.

[15] M. S. Demirsoy, M. S. Sarıkaya, S. Kurnaz, Y. H. El Naser, M. A. Hazar, S. Coşkun, et al., "Enhancing stirring performance through chaotic position control in a magnetic stirrer," Journal of the Brazilian Society of Mechanical Sciences and Engineering, vol. 47, no. 11, p. 580, 2025.

[16] Y. H. El Naser, B. Demirsoy, K. Erin, and M. S. Demirsoy, "Chaotic speed control of a DC motor using the Sprott-A system for robotic end-effector applications," Black Sea Journal of Engineering and Science, vol. 8, no. 5, pp. 1406–1414, 2025.

[17] M. S. Sarıkaya, M. S. Demirsoy, and M. Ç. Kutlu, "Design of a chaotic speed-controlled mixing device and efficiency analysis in biogas," Black Sea Journal of Engineering and Science, vol. 8, no. 3, pp. 672–679, 2025.

[18] H. Gao, H. Zhang, and L. Xiong, "Sliding mode control of Lorenz chaotic system of fluid thermal convection between infinite plates based on LMI," *Advances in Mechanical Engineering*, vol. 15, no. 1, 2023.

[19] S. Vaidyanathan and S. Pakiriswamy, "A 3-D novel conservative chaotic system and its generalized projective synchronization via adaptive control," *Journal of Engineering Science & Technology Review*, vol. 8, no. 2, 2015.

[20] M. Shafiq, I. Ahmad, O. A. Almatroud, and M. M. Al-Sawalha, "Robust attitude control of the three-dimensional unknown chaotic satellite system," *Transactions of the Institute of Measurement and Control*, vol. 44, no. 7, pp. 1484–1504, 2022.

[21] X. Lu, "A financial chaotic system control method based on intermittent controller," *Mathematical Problems in Engineering*, vol. 2020, Article ID 5810707, 2020.

[22] H. Tian, M. Zhao, J. Liu, Q. Wang, X. Yu, and Z. Wang, "Dynamic analysis and sliding mode synchronization control of chaotic systems with conditional symmetric fractional-order memristors," *Fractal and Fractional*, vol. 8, no. 6, p. 307, 2024.

[23] L. Xiong, Y. J. Lu, Y. F. Zhang, X. G. Zhang, and P. Gupta, "Design and hardware implementation of a new chaotic secure communication technique," *PLoS ONE*, vol. 11, no. 8, p. e0158348, 2016.

[24] J. Petrzela, "Chaos in analog electronic circuits: Comprehensive review, solved problems, open topics and small example," *Mathematics*, vol. 10, no. 21, p. 4108, 2022.

[25] J. Zheng, Q. Zhang, Q. Xu, F. Xu, and V. Shi, "Synchronization of a supply chain model with four chaotic attractors," *Discrete Dynamics in Nature and Society*, vol. 2022, Article ID 6390456, 2022.

[26] A. Biswas, S. S. Chaurasia, P. Parmananda, and S. Sinha, "Asymmetry induced suppression of chaos," *Scientific Reports*, vol. 10, no. 1, p. 15582, 2020.

[27] H. P. Ren, C. Bai, K. Tian, and C. Grebogi, "Dynamics of delay induced composite multi-scroll attractor and its application in encryption," *International Journal of Non-Linear Mechanics*, vol. 94, pp. 334–342, 2017.

[28] Y. Ye and J. He, "Constructing a new multi-scroll chaotic system and its circuit design," *Mathematics*, vol. 12, no. 13, p. 1931, 2024.

[29] W. Gao and J. C. Hung, "Variable structure control of nonlinear systems: A new approach," *IEEE Transactions on Industrial Electronics*, vol. 40, no. 1, pp. 45–55, 1993.

[30] M. S. Sarıkaya, O. Demirel, S. Kaçar, and A. Derdiyok, "Modelling and chaotic based parameter optimization of sliding mode controller," *Journal of Mathematical Sciences and Modelling*, vol. 8, no. 2, pp. 42–55, 2025.